

1 **Capturing intrahost recombination of SARS-CoV-2 during superinfection with Alpha and**
2 **Epsilon variants in New York City**

3
4 Authors: Joel O. Wertheim^{1,*}, Jade C. Wang^{2,*}, Mindy Leelawong², Darren P. Martin³, Jennifer
5 L. Havens⁴, Moinuddin A. Chowdhury², Jonathan Pekar⁴, Helly Amin², Anthony Arroyo², Gordon
6 A. Awandare⁵, Hoi Yan Chow², Edimarlyn Gonzalez², Elizabeth Luoma⁶, Collins M. Morang'a⁵,
7 Anton Nekrutenko⁷, Stephen D. Shank⁸, Peter K. Quashie⁵, Jennifer L. Rakeman², Victoria
8 Ruiz², Lucia V. Torian², Tetyana I. Vasylyeva¹, Sergei L. Kosakovsky Pond⁸, and Scott Hughes²

9
10 ¹ Department of Medicine, University of California San Diego, La Jolla, CA, USA

11 ² New York City Public Health Laboratory, New York City Department of Health and Mental
12 Hygiene, New York, NY, USA

13 ³ Institute of Infectious Diseases and Molecular Medicine, University of Cape Town, Cape Town,
14 South Africa

15 ⁴ Bioinformatics and Systems Biology Graduate Program, University of California San Diego, La
16 Jolla, CA, US

17 ⁵ West African Centre for Cell Biology of Infectious Pathogens (WACCBIP), University of Ghana,
18 Accra, Ghana

19 ⁶ Bureau of the Communicable Diseases, New York City Department of Health and Mental
20 Hygiene, Long Island City, NY, USA

21 ⁷ Department of Biochemistry and Molecular Biology, The Pennsylvania State University, State
22 College, PA, USA

23 ⁸ Department of Biology, Temple University, Philadelphia, PA USA

24

25 *These authors contributed equally to this work

26

27 To whom correspondence should be addressed: jwertheim@health.ucsd.edu;

28 jwang7@health.nyc.gov

29

30 **ABSTRACT**

31
32 Recombination is an evolutionary process by which many pathogens generate diversity and
33 acquire novel functions. Although a common occurrence during coronavirus replication,
34 recombination can only be detected when two genetically distinct viruses contemporaneously
35 infect the same host. Here, we identify an instance of SARS-CoV-2 superinfection, whereby an
36 individual was simultaneously infected with two distinct viral variants: Alpha (B.1.1.7) and
37 Epsilon (B.1.429). This superinfection was first noted when an Alpha genome sequence failed to
38 exhibit the classic S gene target failure behavior used to track this variant. Full genome
39 sequencing from four independent extracts revealed that Alpha variant alleles comprised
40 between 70-80% of the genomes, whereas the Epsilon variant alleles comprised between 20-
41 30% of the sample. Further investigation revealed the presence of numerous recombinant
42 haplotypes spanning the genome, specifically in the spike, nucleocapsid, and ORF 8 coding
43 regions. These findings support the potential for recombination to reshape SARS-CoV-2 genetic
44 diversity.

45 INTRODUCTION

46
47 Recombination is a common evolutionary feature of positive-strand RNA viruses¹. It can
48 increase genetic diversity and accelerate adaptation in viral populations by combining existing
49 linked allelic variation. The signature of frequent recombination is pervasive across
50 Betacoronaviruses in bats and other animal²⁻⁶ hosts, and its detection is made easier in part by
51 the substantial genetic divergence separating these various coronaviruses. When an individual
52 is simultaneously infected with two genetically distinct strains of a virus, so-called superinfection
53 ⁷, these viruses can recombine to produce a virus with novel allelic combinations. Although
54 recombination is expected to regularly occur during SARS-CoV-2 infections, it can be difficult to
55 detect *in vivo* unless it involves genetically distinguishable parental strains: recombination
56 between two identical or nearly identical genomes leaves no detectable molecular trace.
57 Furthermore, as with influenza virus^{8,9}, SARS-CoV-2 superinfections have been only rarely
58 reported in humans¹⁰⁻¹², likely due to the short mean duration of SARS-CoV-2 infections.

59
60 Early claims of recombination in SARS-CoV-2¹³ may have been confounded by sequencing
61 errors or convergent evolution¹⁴. As the COVID-19 pandemic progressed, and genetically
62 divergent lineages have evolved, evidence for recombination between these lineages is
63 becoming more convincing^{15,16}. Many of these divergent lineages include highly transmissible
64 variants distinguished by S genes that, under positive selection, have accumulated multiple
65 mutations associated with increased transmissibility, virulence, and immune escape^{17,18}.

66
67 Here, we provide a detailed characterization of an instance of superinfection from January 2021,
68 identified by the New York City (NYC) Department of Health and Mental Hygiene (DOHMH). We
69 show that this individual was superinfected with two SARS-CoV-2 variants: Alpha (B.1.1.7) and
70 Epsilon (B.1.429)^{19,20}. Further, we characterize evidence for recombination occurring within this
71 superinfected individual, providing an *in vivo* snapshot of this evolutionary process within SARS-
72 CoV-2.

73 74 RESULTS

75
76 **Patient epidemiology.** In December 2020, researchers and public health officials in the United
77 Kingdom identified a rapidly spreading SARS-CoV-2 variant within England, then designated as
78 PANGO lineage B.1.1.7²⁰, now designated as the Alpha variant of concern in the WHO
79 nomenclature. In NYC, a SARS-CoV-2 genome sequence classified as belonging to the Alpha
80 lineage was obtained from a sample drawn on 4 January 2021 (the 'index case'). Due to the
81 potential public health importance of Alpha variant cases in NYC in early 2021, NYC DOHMH
82 conducted a public health investigation related to the individual from which this sample had
83 been obtained: NYCPHL-002130 (GISAID accession number *EPI_ISL_857200*). This
84 investigation determined that the individual had recently traveled to Ghana (late December/early
85 January), and contact tracing identified another case of an Alpha variant infection, sampled on
86 14 January 2021, in a named contact with a similar travel history (the 'named contact partner'):
87 NYCPHL-002461 (GISAID accession *EPI_ISL_883324*).

88

89 **Atypical Alpha (B.1.1.7) variant PCR screening.** Typical of the Alpha variant ²⁰, NYCPHL-
90 002130 exhibited S gene target failure (SGTF) phenotype with the TaqPath COVID-19 RT-PCR
91 assay (Table 1). NYC PHL uses the ARTIC amplicon-based protocol V3 to sequence full viral
92 genomes and capture intrahost diversity. The viral genome from this index case showed limited
93 intrahost viral diversity (Figure 1). A single variable site was found at position 23099, with C in
94 20.4% of reads and A in 79.6% of reads. All other substitutions differentiating this sequence
95 from the Wuhan-Hu-1 reference genome sequence (*NC_045512.2*) were present in >99.0% of
96 reads.

97
98 During the initial PCR screening of the sample collected from the named contact partner
99 (NYCPHL-002461), the SGTF characteristic of the Alpha variant was not observed (Table 1).
100 Furthermore, genome sequencing revealed substantial intrahost viral diversity within the viral
101 genome, a possible signature of superinfection (Figure 1). To confirm that this intrahost diversity
102 was not attributable to experimental or sequencing artifacts, the original sample was re-
103 extracted and re-sequenced (NYCPHL-002461-B) and similar SGTF was observed. Additional
104 extractions were then performed in duplicate from the original stock (NYCPHL-002461-C and -
105 D) and sequenced. The same signature of intrahost diversity was confirmed in all four
106 sequenced extractions. Four nucleotide (nt) substitutions differentiating this sequence from the
107 reference genome were identified at >90% frequency: C241T, C3037T, C14408T, and
108 A23403G. Numerous additional substitutions, including A23063T (S N501Y), were present, but
109 at slightly lower frequencies. Nonetheless, this genome was classified as an Alpha variant.
110 Notably, the $\Delta 69/70$ and $\Delta 144$ deletions were found at >95% in the sequencing reads, despite
111 the lack of SGTF.

112
113 NYCPHL-002461-A, -B, and -D extracts exhibited low Ct values for the ORF1ab and N gene
114 targets, ranging between 15 and 16 (Table 1). The S gene target Ct values were around 2 to 3
115 cycles higher. The difference suggests a reduction of viral template in the S gene target region,
116 but not SGTF. We note NYCPHL-002461-C yielded an invalid result, as the TaqPath assay
117 showed no amplification on all targets, including the MS2 phage extraction-control target.

118
119 **Intrahost diversity.** The presence of multiple intermediate frequency alleles and the lack of
120 SGTF in the TaqPath assay prompted us to investigate the intrahost diversity in the named
121 contact partner, NYCPHL-002461. Major and minor intrahost strains were distinguished using
122 the previously described and validated Galaxy SARS-CoV-2 allelic variation pipeline ²¹.

123
124 The four replicate sequencing runs for NYCPHL-002461 yielded remarkably similar patterns
125 with allelic frequencies segregating into four categories: shared, major strain, minor strain and
126 other (see Figure 1, interactive notebook at <https://observablehq.com/@spond/nyc-superinfection>). Shared alleles were those present at 90% allele frequency (AF) in three or more
127 samples. The four shared alleles constituting substitution mutations are the same substitutions
128 that define the ancestor of the Lineage B viruses circulating in the United States: C241T,
129 C3037T, C14408T, A23403G (Figure 1; Supplementary Table 1). Two deletions in the S gene
130 ($\Delta 69-70$ and $\Delta 144$) were also present at high AF (>97%).
131
132

133 Major strain alleles are those that occurred at frequencies between 60 and 90% (≥ 3 samples),
134 with all diagnostic Alpha mutations in this set. Minor strain alleles are those that occurred at
135 frequencies between 10 and 25% (≥ 3 samples), with all but one diagnostic Epsilon mutation in
136 this set; the A28272T mutation characteristic of Epsilon is absent in NYCPHL-002461. Notably,
137 the “other” category encompasses all other variable sites, i.e. those occurring at AF between
138 25% and 60% or those found in only one or two samples. The two alleles were found in all four
139 replicate sequences at intermediate frequencies: G7723A (30.3%) and C23099A (46.7%).
140 These frequencies are suggestive of intrahost variation in the major strain.

141
142 In contrast, the sequencing dataset for the index case, NYCPHL-002130, showed all but one of
143 the alleles occurring at $\geq 85\%$, and all but one of the alleles (C14676T) were also found as
144 “shared” or “major strain” classes in the NYCPHL-002461 datasets (Figure 1). The C23099A
145 mutation, which was at intermediate frequency in NYCPHL-002461, was present at only 88.1%
146 in NYCPHL-002130 from the index case, suggesting the transmission of a mixed viral
147 population between these individuals.

148
149 **Phylogenetic inference with major and minor variants.** We identified sub-clades within
150 Alpha and Epsilon that shared substitutions with the major and minor strains (Figure 2). We
151 inferred a maximum likelihood (ML) phylogenetic tree in IQTree2 for the major strain and 1174
152 related B.1.1.7 genomes containing the C2110T, C14120T, C19390T, and T7984C substitutions
153 found in the major strain (Figure 2A). We also inferred an ML tree for the minor strain and 807
154 related B.1.429 genomes containing the C8947T, C12100T, and C10641T substitutions found in
155 the minor strain (Figure 2C).

156
157 Root-to-tip regression analyses show that the NYCPHL-002461 sampling date is consistent with
158 the molecular clock for both the major and minor strain sequences (Figure 2B/2D), indicating
159 that one would expect viruses of this degree of genetic divergence to have been circulating in
160 mid-January 2021. In fact, genomes identical to the major variant were sampled in both NYC
161 (the NYCPHL-002130 index case) and in Ghana (EPI_ISL_944711) on 8 January 2021,
162 consistent with a scenario in which this particular Alpha virus was introduced into NYC by an
163 individual who had recently traveled to Ghana and had contact with the named contact partner.
164 These three viruses share a common ancestor around 4 January 2021 and are separated by
165 additional viruses sampled in Ghana by two mutations: C912T and C23099A. Notably, the latter
166 mutation appears at intermediate frequency in both NYCPHL-002130 and NYCPHL-002461.

167
168 The minor variant is genetically distinct from all other sampled genomes, including any genome
169 sequenced by NYC DOHMH (Figure 2C). The closest relatives were sampled in California
170 (EPI_ISL_3316023, EPI_ILS_1254173, EPI_ISL_2825578), the United Kingdom
171 (EPI_ILS_873881), and Cameroon (EPI_ISL_1790107, EPI_ISL_1790108, EPI_ISL_1790109).
172 The most similar of these relatives is EPI_ISL_3316023, which was sampled on 11 January
173 2021 in California and represents the direct ancestor of the minor variant on the phylogeny. The
174 only mutation separating these genomes is T28272A, which is a reversion away from an
175 Epsilon-defining mutation. There are no sequenced closely related Epsilon genomes from NYC,

176 although this variant was present at a prevalence around 1% in NYC during the first two weeks
177 of 2021 in NYC ²².

178
179 **Four-gamete tests of recombination.** A preliminary inquiry of the genome sequencing data
180 from the S (12 contiguous read fragments) and nucleoprotein (3 contiguous read fragments)
181 regions was suggestive of recombinant genome fragments within the named contact partner. To
182 determine whether pairs of polymorphic sites within individual read fragments displayed
183 evidence of recombination we employed three different four-gamete based recombination
184 detection tests: PHI ²³, MCL, and R² vs Dist ²⁴ (Table 2). The power of each of these tests to
185 detect recombination was seriously constrained by the short lengths of the read fragments and
186 the low numbers of both variant-defining sites and other polymorphic sites with minor allele
187 frequencies >1% within each of the fragments. Only three of the 15 read fragments (read
188 fragments 6 and 8 in the S-gene and read fragment 3 in the N-gene) encompassed two or more
189 of the variant-defining sites that were expected to provide the best opportunities to detect
190 recombination. Nevertheless, pairs of sites within four read fragments in the S gene (positions
191 23123–24467 covering fragments 7, 8, 9 and 10) and one read fragment in the nucleoprotein
192 gene (positions 28986–29378 covering fragment 3) exhibited signals of significant phylogenetic
193 incompatibility with at least two of the three tests ($p < 0.05$): signals which are consistent with
194 recombination. The only read fragment for which evidence of recombination was supported by
195 all three tests was fragment 3 in the N-gene: a fragment that was one among only three that
196 contained multiple variant-defining sites. Eight of the fifteen analyzed read-fragment alignments
197 exhibited no signals of recombination using any of the tests, which is unsurprising given the lack
198 within these fragments of both variant-defining substitutions and polymorphic sites with minor
199 allele frequencies greater than 1%.

200
201 **Targeted sequencing for recombination detection.** The four gamete tests on genomic
202 sequencing data is limited by the short length of amplified fragments. To obtain data from longer
203 sequence fragments, we PCR-amplified three regions of the genome from the original nucleic
204 acid extracts, cloned them, and then sequenced individual clones. These longer genomic
205 fragments provide greater resolution for detecting recombination, compared with the short
206 fragments from deep sequencing analysis, because they include more differentiating sites
207 spread out farther across the genome.

208
209 The longest cloned region spanned 947 nt within the S gene and contained 5 nt substitutions
210 differentiating the major and minor strains plus a variable site in the major variant. Of the 104
211 clones sequenced within this region, 60 (57.7%) were major strain haplotypes, 13 (12.5%) were
212 minor strain haplotypes, whereas the remaining 31 clones (29.8%) contained both major and
213 minor strain mutations, consistent with recombination (Figure 3A). We observed 11 distinct
214 combinations of major and minor strain mutations across these clones, with two distinct
215 haplotypes present in 6 clones apiece. Most haplotypes are consistent with only a single
216 recombination breakpoint, though we did observe clones consistent with 2 or 3 breakpoints.

217
218 The second cloned S region spanned 658 nt in S including the Δ 69-70 and Δ 144 deletions
219 characteristic of the major strain and two 2 substitutions in the minor strain. Of the 93 clones

220 sequenced, 69 (74.1%) were major strain haplotypes, 17 (18.3%) were minor strain haplotypes,
221 and 7 (7.5%) were mixed haplotypes (Figure 3B). Five of these mixed haplotypes contained
222 only one of the two deletions. Unlike in the primary sequencing analyses where the $\Delta 69-70$ and
223 $\Delta 144$ deletions were present in >98% of sequences, $\Delta 69-70$ was observed in only 72 (77.4%)
224 clones and $\Delta 144$ was observed in only 71 (76.3%). These frequencies are consistent with the
225 frequency of the other major strain substitutions in the primary sequencing analysis.

226
227 The third, and shortest, cloned region spanned 476 nt of ORF8, surrounding 4 substitutions
228 defining the major strain and 1 minor strain substitution. Of the 36 cloned sequences, 30
229 (83.3%) had the major strain haplotype, 2 (5.6%) had the minor variant haplotype, and 4
230 (11.1%) had mixed haplotypes consistent with recombination (Figure 3C). Notable, the
231 discriminating substitutions only span 223 nt of this region.

232
233 **Consistency between cloning and genome sequencing analyses.** *In-vitro* recombination
234 can be introduced by reverse-transcription and PCR amplification, which are part of both
235 genome sequencing and cloning protocols²⁵. These *in-vitro* effects have a strong stochastic
236 component and would result in substantially different recombinant haplotype frequencies across
237 different extracts and PCR experiments. To determine the extent to which these protocols could
238 have led to biased inference of recombination, we compared the haplotype frequencies across
239 the four extracts from NYCPHL-002461, which had each independently been subjected to
240 reverse transcription and PCR amplification, and the frequency of these haplotypes in the
241 cloning experiment, which included PCR amplification.

242
243 Within the S gene substitution region encompassing nucleotide positions 23604–23709, the
244 major haplotype was present between 76.4% and 78.6%, and the minor haplotype was between
245 13.7% and 15.4% (Supplementary Table 1). The recombinant haplotype positions 23604A and
246 23709C was present at 3.9% allele frequency (standard deviation of 0.34% across extracts),
247 whereas recombinant haplotype 23604C and 23709T was present at 4.3% (standard deviation
248 of 0.37% across extracts). Although the haplotype frequencies among extracts were significantly
249 different ($p=0.029$; chi-square test), the magnitude of these differences were unremarkable.
250 Furthermore, there was no significant difference between the frequency of these haplotypes in
251 cloning experiment and extracts ($p=0.190$ versus -A; $p=0.189$ versus -B; $p=0.357$ versus -C;
252 $p=0.206$ versus -D; Fisher's Exact Test).

253
254 A similar pattern was observed within the ORF8 region at nucleotide positions 27972–28111,
255 which included four discrimination sites: 27972, 28048, 28095, and 28111 (Supplementary
256 Table 2). The predominant recombinant haplotypes were consistent across the four extracts,
257 and the frequencies differed only slightly ($p=0.077$; chi-square test). As in S, the frequency of
258 these recombinant haplotypes in the cloning experiment was not significantly different from any
259 of the extracts ($p=0.405$ versus -A; $p=0.413$ versus -B; $p=0.199$ versus -C; $p=0.408$ versus -D;
260 Fisher's exact test).

261

262 Hence, *in-vitro* recombination induced by either reverse-transcription or PCR amplification, does
263 not appear to have been the dominant contributor to the recombinant haplotype distribution
264 reported here.

265
266 **Search for transmission of a circulating recombinant.** To determine whether there was
267 onward transmission of a recombinant descendent of these major and minor strains, we queried
268 the 27,806 genomes sequenced by NYC public health surveillance and deposited to GISAID
269 through 05 September 2021. We tested these genomes for mosaicism (3SEQ; ²⁶; with Dunn-
270 Sidak correction for multiple comparisons) of the major and minor strains; however, we were
271 unable to reject the null hypothesis of non-reticulate evolution for any of these genomes. There
272 is no evidence of an Alpha/Epsilon recombinant that circulated in New York City.

273
274 Since the Dunn-Sidak correction done in the 3SEQ analysis applies a conservative type-1 error
275 threshold of 0.05, we reran the analysis using a more permissive threshold of 0.25 (see
276 methods) and were able to reject the null hypothesis for a single genome (EPI_ISL_2965250;
277 $p=2.24 \times 10^{-6}$ and Dunn-Sidak corrected $p=0.117$). Although this genome contains many of the
278 mutations characteristic of the Alpha variant throughout the genome, it does not possess
279 mutations unique to the major strain nor any Epsilon-specific mutations. Rather, within the
280 putative recombinant regions, the EPI_ISL_2965250 genome has C8809T, C27925T, C28311T,
281 and T28879G. All of these mutations are characteristic of the B.1.526 Iota-variant, prevalent in
282 NYC in early 2021. Therefore, this genome is likely not a descendant of the major and minor
283 strains. Instead it appears to be a recombinant descendant of Alpha and Iota viruses.

284 285 **DISCUSSION**

286
287 Here, we report evidence of intra-host recombination of SARS-CoV-2 within a single individual
288 superinfected with Alpha and Epsilon viral variants during the second COVID-19 wave in New
289 York City in early 2021. Because recombinant viruses can be successfully generated and
290 transmitted¹⁵ between humans, this finding underscores their potential relevance to the future of
291 the COVID-19 pandemic.

292
293 The presence of major and minor strains described within the superinfected individual are
294 unlikely to be the result of bioinformatics error, contamination, or experimental artifacts. The
295 degree of evolutionary divergence of each of the strains from other available SARS-CoV-2
296 genomes is consistent with viruses circulating at the time of their January 2021 sampling dates.
297 Moreover, the major strain genome is identical to contemporaneously sampled genomes from
298 both a named contact and strains circulating in the country from which they had both recently
299 visited. No closely related genome to the minor strain was ever sequenced by NYC DOHMH,
300 lessening the probability of a contaminated sample. Given the relatively low sequencing
301 coverage in NYC in January 2021 and low prevalence of the Epsilon variant, around 1% in NYC
302 at the time, it is not unexpected that a closely related genome would not be observed.
303 Furthermore, the major and minor variants were both present in all four extractions of the two
304 aliquots at similar frequencies, indicating that any contamination, if present, would need to have
305 occurred in the original sample swab.

306

307 The timing of this superinfection is important, because January 2021 was the peak of the
308 second COVID-19 wave in NYC, a time when numerous variants were circulating and
309 immediately prior to the vaccination roll-out campaign. Hence, January 2021 in NYC represents
310 not only the height of potential for superinfection risk, but also a location where its existence
311 would be most apparent due to the co-circulation of numerous genetically distinct viral variants.

312

313 There remain unexplained patterns in the genome sequencing data from the superinfected
314 individual. Evidence of a major and minor strain was not apparent at the S deletions $\Delta 69/70$ and
315 $\Delta 144$ in the genome sequencing, but the cloning analysis showed major and minor alleles at
316 these sites at the expected frequencies. Therefore, it is possible that the ARTIC protocol
317 preferentially sequenced templates containing these deletions, giving a false impression of their
318 predominance in the genomic analysis. Also of interest is the A28272T mutation in the minor
319 strain, which is either a reversion or potential sequencing artifact. If the base-call at position
320 28272 in the minor variant is erroneous, then the minor strain would be identical to a virus
321 sampled contemporaneously in California, where the Epsilon variant was first discovered and
322 likely originated.

323

324 Laboratory induced recombination is a common artifact during reverse-transcription and PCR
325 ^{27,28}. However, recombination is a pervasive feature of natural coronavirus infection, as it has
326 been observed in bats, camels, and humans ^{2,15,29,30}. One would *a priori* expect to find
327 recombinant viruses in a SARS-CoV-2 superinfected individual. Therefore, it is unlikely that the
328 entirety of the signal for recombination reported here is due to reverse-transcription or PCR-
329 induced recombination. A consistent signal for recombination was observed in the four whole
330 genome sequencing analyses and in cloned-fragment analysis, all suggesting the same
331 recombinant haplotypes present at high frequency.

332

333 Our search for Alpha/Epsilon variant recombinants in NYC did not identify genomes that would
334 suggest onward transmission of either of the major or minor strains derived here, or a
335 recombinant offspring. This lack of onward transmission is not surprising, given that the initial
336 index case was contacted by NYC DOHMH personnel and their named contact (the
337 superinfected case) received a prompt COVID-19 diagnosis and was advised to self-isolate.

338

339 It is likely that superinfection with SARS-CoV-2 is more common than has been described in the
340 literature, especially given the documentation of circulating recombinant strains of the Alpha
341 variant in the United Kingdom ¹⁵. Recombinant virus can only be produced within a
342 superinfected individual. That said, we caution against assuming superinfection before potential
343 issues of contamination, poor-quality sequencing, or bioinformatics errors have been
344 appropriately dealt with.

345

346 The high number and genomic variability recombinant haplotypes that we have identified within
347 a single superinfected individual suggests that recombination is perpetually occurring within
348 SARS-CoV-2 infections. Whether recombination will play a role in the emergence of novel
349 SARS-CoV-2 variants is an open question. Reduced incidence due to vaccine-induced and

350 naturally-acquired immunity would lower the opportunity for superinfection, and the
351 homogenizing effect of variant-driven selective sweeps (as seen in the Delta and Omicron
352 variants ³¹) will lessen the potential for biological innovation in a recombinant genome.
353 Nonetheless, SARS-CoV-2 molecular surveillance should actively monitor for the emergence of
354 a recombinant variant.
355
356

357 MATERIALS AND METHODS

358

359 **Extraction and sequencing.** Nasopharyngeal specimens positive for SARS-CoV-2 with Ct < 32
360 were submitted to NYC PHL for sequence analysis by the NYC DOHMH through the COVID
361 Express clinics. The NYCPHL-002130 and -002461 specimens had Ct values of 19 and 20
362 cycles, respectively, which allowed for sequencing at NYC PHL. Each specimen was split into
363 separate extraction and archive aliquots. Nucleic acid extraction was performed using the
364 KingFisher Flex Purification System (Thermo Fisher Scientific) from the extraction aliquot.
365 Eleven μ L of extract was used to anneal with random hexamers and dNTPs (New England
366 Biolabs Inc., NEB) and reverse transcribed with SuperScript IV Reverse Transcriptase at 42 °C
367 for 50 min. The cDNA product was amplified in two separate multiplex PCRs with ARTIC V3
368 primer pools (Integrated DNA Technologies) in the presence of Q5 2x Hot Start Master Mix
369 (NEB) at 98 °C for 30 s, and 35 cycles of 98 °C for 15 s and 65 °C for 5 min. The two PCR
370 products were combined and were purified with Agencourt Ampure XP magnetic beads
371 (Beckman Coulter) at a 1:1 sample-to-bead ratio. The bead-cleaned PCR products were
372 quantified using a Qubit 3.0 fluorometer (Thermo Fisher Scientific). Standard protocol was used
373 for library preparation in the NEBNext Ultra II Library Preparation workflow using 90 ng of PCR
374 product (NEB). In short, the ARTIC PCR products were used in an end-repair reaction, which
375 added a 5'-phosphate group and a dA-tail, in a reaction for 30 min at 20 °C. The reaction was
376 heat inactivated for 30 min at 65 °C. NEBNext Adaptor was ligated at 25 °C for 30 min and
377 cleaved by USER Enzyme at 37 °C for 15 min. The product was Agencourt Ampure XP bead-
378 purified at a ratio of 0.6x sample:beads. The bead-cleaned, end-ligated amplicons were
379 subjected to a 6-cycle PCR reaction with NEBNext Ultra II Q5 Master Mix in the presence of
380 NEBNext Multiplex Oligos for Illumina (NEB), which added a sample-specific 8-base index and
381 Illumina P5 and P7 adapters for sequencing on Illumina instruments. The product was purified
382 with Ampure XP beads at a 0.6x sample:bead ratio and quantified, normalized and pooled at
383 equimolar concentration with other libraries, followed by loading onto the Illumina MiSeq
384 sequencing instrument using V3 600-cycle reagent kit, with a V3 flow cell for 250-cycle paired-
385 end sequencing (Illumina). For NYCPHL-002461, the same “extraction” specimen aliquot was
386 used for a second extraction, Extract B. Extracts C and D were independent extractions, but
387 from the “archived” specimen aliquot. As such, the first extract (A), and extracts B, C, and D
388 were independent samples which underwent independent reverse transcription, ARTIC PCR,
389 library preparation, and sequencing reactions.

390

391 Potential *in vitro* recombination that occurred during the four independent extractions, reverse-
392 transcription reactions, and library preparation procedures, such as PCR amplification, would
393 require the events to occur independently at the same stage four times in order to produce the
394 same proportions of Major and Minor variant haplotypes in the high-throughput sequencing
395 data. To account for *in vitro* recombination, regions where long complete reads span across
396 major and minor variants in close proximity, <105 nucleotide bases, were examined across all
397 genome alignments of the four NYCPHL-002461 replicates. Reads with SAM (Sequence
398 Alignment Map) Flags 81,83,97,113,145,147,161,177,2129 are included in the analysis. Reads
399 with other flags are excluded from the analysis or are not found in the alignment files.
400 Additionally, reads without a combination of major or minor alleles are excluded. All unique

401 haplotypes at major and minor variant positions are grouped together. Relative frequencies of
402 the haplotypes are calculated for each region of all four extractions.

403
404
405 **Cloning.** Three regions of the SARS-CoV-2 genome from NYCPHL-002461 were cloned. Two
406 contained non-overlapping regions of the S gene and were designated S_Sub (positions
407 22882–23873) and S_Del (positions 21421–22098). The third region included part of the ORF8
408 gene (positions 27798–28280).

409
410 To perform the annealing step for reverse transcription, 3 µl of the NYCPHL-002461 nucleic
411 acid extract was combined with reverse primer and dNTPs at final concentrations of 154 nM and
412 769 µM, respectively. Annealing was performed by heating to 65°C for 5 minutes then cooling to
413 4°C. The reverse primer sequences used for the reverse transcription are as follows: S_Sub
414 primer-R is 5'-CTATTCCAGTTAAAGCACGGTTT, S_Del is 5'-
415 AGGTCCATAAGAAAAGGCTGAGA and ORF8 is 5'-GAGACATTTAGTTTGTTCGTTTA. An
416 elongation mix containing 200 units of SuperScript IV Reverse Transcriptase (Invitrogen) and 40
417 units of RNaseOUT Recombinant Ribonuclease Inhibitor (Invitrogen) was then added along with
418 dNTPs at a final concentration of 200 µM. The resulting solution was heated to 55°C for 10
419 minutes then 80°C for 10 minutes.

420 Each cDNA target was PCR amplified using Platinum II Taq polymerase and its accompanying
421 buffer (Invitrogen) supplemented with a final concentration of 200 µM dNTPs and 600 nM of
422 each primer. The reverse primer sequences used for reverse transcription were included along
423 with their corresponding forward primers: S_Sub primer-F is 5'-
424 TCTTGATTCTAAGGTTGGTGGT, S_del is 5'-AGGGGTAAGTCTGTTATGTCT and ORF8 is
425 5'-GCCTTTCTGCTATTCCTTGT. PCR was performed with the following cycling conditions: an
426 initial hold at 94°C for 2 minutes, followed by 35 cycles at 94°C for 15 seconds, 60°C for 15
427 seconds and 68°C for 15 seconds. Cycling was followed by a final extension step at 72°C for 7
428 minutes. The PCR products were run on 2% agarose gels, excised and gel purified with the
429 GenElute Gel Extraction Kit (Sigma). The gel-purified PCR products were cloned using the
430 TOPO TA Cloning Kit for Sequencing (Invitrogen).

431 Individual colonies resulting from the transformation into chemically competent One Shot
432 TOP10 *Escherichia coli* (Invitrogen) were picked and patch plated for sequencing. Rolling circle
433 amplification and Sanger sequencing of the clones were performed by GeneWiz (New Jersey).
434 All clones were sequenced with the M13 reverse primer. Due to its larger size, S_Sub clones
435 were also sequenced with the M13 forward primer.

436 **Major and minor variant calling.** We used the Galaxy SARS-CoV-2 variant calling pipeline for
437 paired-end Illumina ARTIC amplicon data²¹. Briefly, the workflow performs quality control,
438 masks primer sites, maps reads to reference using *BMA-mem*, calls variants using *lofreq*,
439 annotates them using *SNPEff*, and outputs tabular variant call files, thresholded on minimum
440 allele frequency of 0.05. These variants are further visualized in a custom ObservableHQ
441 notebook (<https://observablehq.com/@spond/nyc-superinfection>).

442

443 **Alignment and phylogenetic inference.** SARS-CoV-2 genomes were downloaded from
444 GISAID on 24 March 2021. Genomes assigned to the B.1.1.7 or B.1.429 Pangolin lineage³²
445 were aligned to the Wuhan-Hu-1 reference genome using the --6merpair option in Mafft v7.464
446³³. We further refined these alignments to only those genomes sharing specific synapomorphies
447 with the major and minor allelic variants from NYCPHL-002461: C241T, C3037T, C14408T, and
448 A23403G for B.1.1.7 viruses and C8947T, C12110T, and C10641T for B.1.429 viruses.
449 Separate maximum likelihood phylogenetic trees for B.1.1.7 (n=1176) and B.1.429 (n=807)
450 were inferred in IQTree2 under a GTR+F+I model, with the additional NNI search option and a
451 minimum branch length of 1e-9 substitutions/site³⁴.

452
453 **Molecular clock inference.** To determine whether the major and minor allelic variants were
454 contemporaneous with the date of sampling, we estimated clock trees for the B.1.1.7 and
455 B.1.429 phylogenies in TreeTime v0.8.0³⁵. We fixed the clock rate to 8×10^{-4}
456 substitutions/site/year under a skyline coalescent model (per NextStrain default parameters for
457 SARS-CoV-2). These trees were also used to estimate the time to most recent common
458 ancestor of the allelic variants and their closest relatives.

459
460 **Four-gamete tests for recombination.** When sequences evolve in the absence of both
461 recombination and convergent mutations it is expected that, for any pair of polymorphic sites
462 where one of the sites has either nucleotide X or Y and the other has either nucleotide A or B,
463 no more than three of the four possible combinations of nucleotides (or gametes) at the two
464 sites (i.e. XA, XB, YA and YB) should ever be observed. Given that in reality convergent
465 mutations are always possible, four gamete tests of recombination attempt to detect situations
466 where the numbers of site pairs where all four combinations of nucleotides are observed exceed
467 that expected due to convergent mutations in the absence of recombination. We tested 15
468 multiple sequence alignments, each containing all observed unique read fragment sequences
469 spanning the S-gene (12 fragments) and N-gene (3 fragments) with three different four gamete
470 tests: (1) the PHI test (implemented in RDP5^{23,36}) which considers sites with more than two
471 alternative nucleotide states and uses a permutation-based test to determine whether detected
472 site pairs displaying all four gametes display a degree of spatial clustering along the sequence
473 that is significantly higher than would be expected in the absence of recombination; (2) the MCL
474 recombination detection test (implemented in the pairwise component of the LDHat package;²⁴)
475 which uses an approximate maximum likelihood method to infer the population scaled
476 recombination rate needed to explain the observed numbers of site pairs with four gametes and
477 then tests for significant deviation of the inferred recombination rate from zero using a
478 permutation test, and (3) the RvsDist test (implemented in pairwise component of LDHat) which
479 determines the correlation between the R^2 measure of linkage disequilibrium between site pairs
480 with four gametes with the physical distance in nucleotides between the site pairs²⁴ and uses a
481 permutation test to detect significant deviations from the expected degree of correlation in the
482 absence of recombination. For both the MCL and RvsDist tests we used a minor allele
483 frequency cutoff of 0.01.

484
485 **Population level recombination detection.** We downloaded all SARS-CoV-2 sequences from
486 GISAID that were deposited by 5 September 2021³⁷ and analyzed the 27,806 genomes

487 sequenced by the NYC PHL and Pandemic Response Lab (PRL) from specimens collected
488 from NYC residents. These genomes were aligned to the Wuhan-Hu-1 reference genome
489 (Genbank accession NC_045512.2) using MAFFT v7.453 (options --auto --keeplength --
490 addfragments)³³.

491
492 To determine whether there was any onward transmission of a major-minor strain recombinant,
493 we used 3SEQ v.1.7²⁶ as a statistical test for recombination in the NYC data. 3SEQ
494 interrogates triplets of sequences for signals of mosaicism in a sequence given two 'parental'
495 sequences. We interrogated each of the 27,806 NYC PHL and PRL-generated genomes for
496 mosaicism given the major and minor strains as parents. The resulting *p*-values are Dunn-Sidak
497 corrected for multiple comparisons ($n=55612$), and we tested for mosaicism at *p*-value
498 thresholds 0.05 and 0.25. The single nucleotide differences between a putative recombinant
499 and the major and minor strains were visualized using snipit
500 (<https://github.com/aineniamh/snipit>).

501

502

503 **Data availability.**

504 The data analyzed as part of this project were obtained from the GISAID database and through
505 a Data Use Agreement between NYC DOHMH and the University of California San Diego. We
506 gratefully acknowledge the authors from the originating laboratories and the submitting
507 laboratories, who generated and shared via GISAID the viral genomic sequence data on which
508 this research is based. A complete list acknowledging the authors who submitted the data
509 analyzed in this study can be found in Data S1.

510
511 Trimmed, host-depleted viral sequencing data and cloned sequence fragments have been
512 submitted to NCBI (accession numbers pending).

513

514 **Acknowledgements.**

515 J.O.W. acknowledges funding from the National Institutes of Health (AI135992 and AI136056).
516 D.P.M was funded by the Wellcome Trust (222574/Z/21/Z). PKQ is funded by a Crick African
517 Network Fellowship. T.I.V. is funded by a Branco Weiss Fellowship. S.L.K.P and A.N were
518 supported in part by a grant from the National Institutes of Health (AI134384). This work was
519 supported (in part) by the Epidemiology and Laboratory Capacity (ELC) for Infectious Diseases
520 Cooperative Agreement (Grant Number: ELC DETECT (6NU50CK000517-01-07) funded by the
521 Centers for Disease Control and Prevention (CDC). Its contents are solely the responsibility of
522 the authors and do not necessarily represent the official views of CDC or the Department of
523 Health and Human Services.

524

525 **Competing interests.**

526 J.O.W. and S.L.K.P has received funding from the CDC (ongoing) via contracts or agreements
527 to their institution unrelated to this research. All other authors declare no competing interests.

528
529
530
531
532
533
534
535
536
537
538
539
540
541
542
543
544
545
546
547
548
549
550
551
552
553
554
555
556
557
558
559
560
561
562
563
564
565
566
567
568
569
570
571
572
573
574
575
576
577
578

REFERENCES

- 1 Worobey, M. & Holmes, E. C. Evolutionary aspects of recombination in RNA viruses. *J Gen Virol* **80** (Pt 10), 2535-2543 (1999).
- 2 Boni, M. F. *et al.* Evolutionary origins of the SARS-CoV-2 sarbecovirus lineage responsible for the COVID-19 pandemic. *Nat Microbiol* **5**, 1408-1417 (2020).
- 3 Liao, C. L. & Lai, M. M. RNA recombination in a coronavirus: recombination between viral genomic RNA and transfected RNA fragments. *J Virol* **66**, 6117-6124 (1992).
- 4 Lytras, S. *et al.* Exploring the natural origins of SARS-CoV-2 in the light of recombination. *bioRxiv* **2021.01.22.427830** (2021).
- 5 Sabir, J. S. *et al.* Co-circulation of three camel coronavirus species and recombination of MERS-CoVs in Saudi Arabia. *Science* **351**, 81-84 (2016).
- 6 Siapco, B. J., Kaplan, B. J., Bernstein, G. S. & Moyer, D. L. Cytodiagnosis of *Candida* organisms in cervical smears. *Acta Cytol* **30**, 477-480 (1986).
- 7 Smith, D. M., Richman, D. D. & Little, S. J. HIV superinfection. *J Infect Dis* **192**, 438-444 (2005).
- 8 Myers, C. A. *et al.* Dual infection of novel influenza viruses A/H1N1 and A/H3N2 in a cluster of Cambodian patients. *Am J Trop Med Hyg* **85**, 961-963 (2011).
- 9 Rith, S. *et al.* Natural co-infection of influenza A/H3N2 and A/H1N1pdm09 viruses resulting in a reassortant A/H3N2 virus. *J Clin Virol* **73**, 108-111 (2015).
- 10 Samoilov, A. E. *et al.* Case report: change of dominant strain during dual SARS-CoV-2 infection. *BMC Infect Dis* **21**, 959 (2021).
- 11 Tarhini, H. *et al.* Long-Term Severe Acute Respiratory Syndrome Coronavirus 2 (SARS-CoV-2) Infectiousness Among Three Immunocompromised Patients: From Prolonged Viral Shedding to SARS-CoV-2 Superinfection. *J Infect Dis* **223**, 1522-1527 (2021).
- 12 Sjaarda, C. P. *et al.* Phylogenomics reveals viral sources, transmission, and potential superinfection in early-stage COVID-19 patients in Ontario, Canada. *Sci Rep* **11**, 3697 (2021).
- 13 Yi, H. 2019 Novel Coronavirus Is Undergoing Active Recombination. *Clin Infect Dis* **71**, 884-887 (2020).
- 14 Wertheim, J. O. A Glimpse Into the Origins of Genetic Diversity in the Severe Acute Respiratory Syndrome Coronavirus 2. *Clin Infect Dis* **71**, 721-722 (2020).
- 15 Jackson, B. *et al.* Generation and transmission of interlineage recombinants in the SARS-CoV-2 pandemic. *Cell* **184**, 5179-5188 e5178 (2021).
- 16 VanInsberghe, D., Neish, A. S., Lowen, A. C. & Koelle, K. Recombinant SARS-CoV-2 genomes are currently circulating at low levels. *bioRxiv* (2021).
- 17 Kustin, T. *et al.* Evidence for increased breakthrough rates of SARS-CoV-2 variants of concern in BNT162b2-mRNA-vaccinated individuals. *Nat Med* **27**, 1379-1384 (2021).
- 18 Martin, D. P. *et al.* The emergence and ongoing convergent evolution of the SARS-CoV-2 N501Y lineages. *Cell* **184**, 5189-5200 e5187 (2021).
- 19 Deng, X. *et al.* Transmission, infectivity, and neutralization of a spike L452R SARS-CoV-2 variant. *Cell* **184**, 3426-3437 e3428 (2021).
- 20 Volz, E. *et al.* Assessing transmissibility of SARS-CoV-2 lineage B.1.1.7 in England. *Nature* **593**, 266-269 (2021).
- 21 Maier, W. *et al.* Ready-to-use public infrastructure for global SARS-CoV-2 monitoring. *Nat Biotechnol* **39**, 1178-1179 (2021).
- 22 West, A. P., Jr. *et al.* Detection and characterization of the SARS-CoV-2 lineage B.1.526 in New York. *Nat Commun* **12**, 4886 (2021).
- 23 Bruen, T. C., Philippe, H. & Bryant, D. A simple and robust statistical test for detecting the presence of recombination. *Genetics* **172**, 2665-2681 (2006).

- 579 24 McVean, G., Awadalla, P. & Fearnhead, P. A coalescent-based method for detecting
580 and estimating recombination from gene sequences. *Genetics* **160**, 1231-1241 (2002).
- 581 25 Gorzer, I., Guelly, C., Trajanoski, S. & Puchhammer-Stockl, E. The impact of PCR-
582 generated recombination on diversity estimation of mixed viral populations by deep
583 sequencing. *J Virol Methods* **169**, 248-252 (2010).
- 584 26 Lam, H. M., Ratmann, O. & Boni, M. F. Improved Algorithmic Complexity for the 3SEQ
585 Recombination Detection Algorithm. *Mol Biol Evol* **35**, 247-251 (2018).
- 586 27 Lenz, T. L. & Becker, S. Simple approach to reduce PCR artefact formation leads to
587 reliable genotyping of MHC and other highly polymorphic loci--implications for
588 evolutionary analysis. *Gene* **427**, 117-123 (2008).
- 589 28 Schlub, T. E., Smyth, R. P., Grimm, A. J., Mak, J. & Davenport, M. P. Accurately
590 measuring recombination between closely related HIV-1 genomes. *PLoS Comput Biol* **6**,
591 e1000766 (2010).
- 592 29 Dudas, G., Carvalho, L. M., Rambaut, A. & Bedford, T. MERS-CoV spillover at the
593 camel-human interface. *Elife* **7** (2018).
- 594 30 Vijgen, L. *et al.* Complete genomic sequence of human coronavirus OC43: molecular
595 clock analysis suggests a relatively recent zoonotic coronavirus transmission event. *J*
596 *Virol* **79**, 1595-1604 (2005).
- 597 31 Mlcochova, P. *et al.* SARS-CoV-2 B.1.617.2 Delta variant replication and immune
598 evasion. *Nature* **599**, 114-119 (2021).
- 599 32 O'Toole, A. *et al.* Assignment of epidemiological lineages in an emerging pandemic
600 using the pangolin tool. *Virus Evol* **7**, veab064 (2021).
- 601 33 Katoh, K. & Standley, D. M. MAFFT multiple sequence alignment software version 7:
602 improvements in performance and usability. *Mol Biol Evol* **30**, 772-780 (2013).
- 603 34 Minh, B. Q. *et al.* IQ-TREE 2: New Models and Efficient Methods for Phylogenetic
604 Inference in the Genomic Era. *Mol Biol Evol* **37**, 1530-1534 (2020).
- 605 35 Sagulenko, P., Puller, V. & Neher, R. A. TreeTime: Maximum-likelihood phylodynamic
606 analysis. *Virus Evol* **4**, vex042 (2018).
- 607 36 Martin, D. P. *et al.* RDP5: a computer program for analyzing recombination in, and
608 removing signals of recombination from, nucleotide sequence datasets. *Virus Evol* **7**,
609 veaa087 (2021).
- 610 37 Shu, Y. & McCauley, J. GISAID: Global initiative on sharing all influenza data - from
611 vision to reality. *Euro Surveill* **22** (2017).
- 612

613 **Table 1. Cycle threshold (Ct) values from TaqPath assays from index case (NYCPHL-**
614 **002130) and named contact partner (NYCPHL-002461).**

615

Case	WGS ID	Ct value		
		ORF1ab	N gene	S gene
Index case	NYCPHL-002130	14.97	15.44	N/A
Named contact partner	NYCPHL-002461-A	14.86	15.70	17.34
	NYCPHL-002461-B	16.06	16.251	18.68
	NYCPHL-002461-C	N/A	N/A	N/A
	NYCPHL-002461-D	15.73	15.83	18.35

616

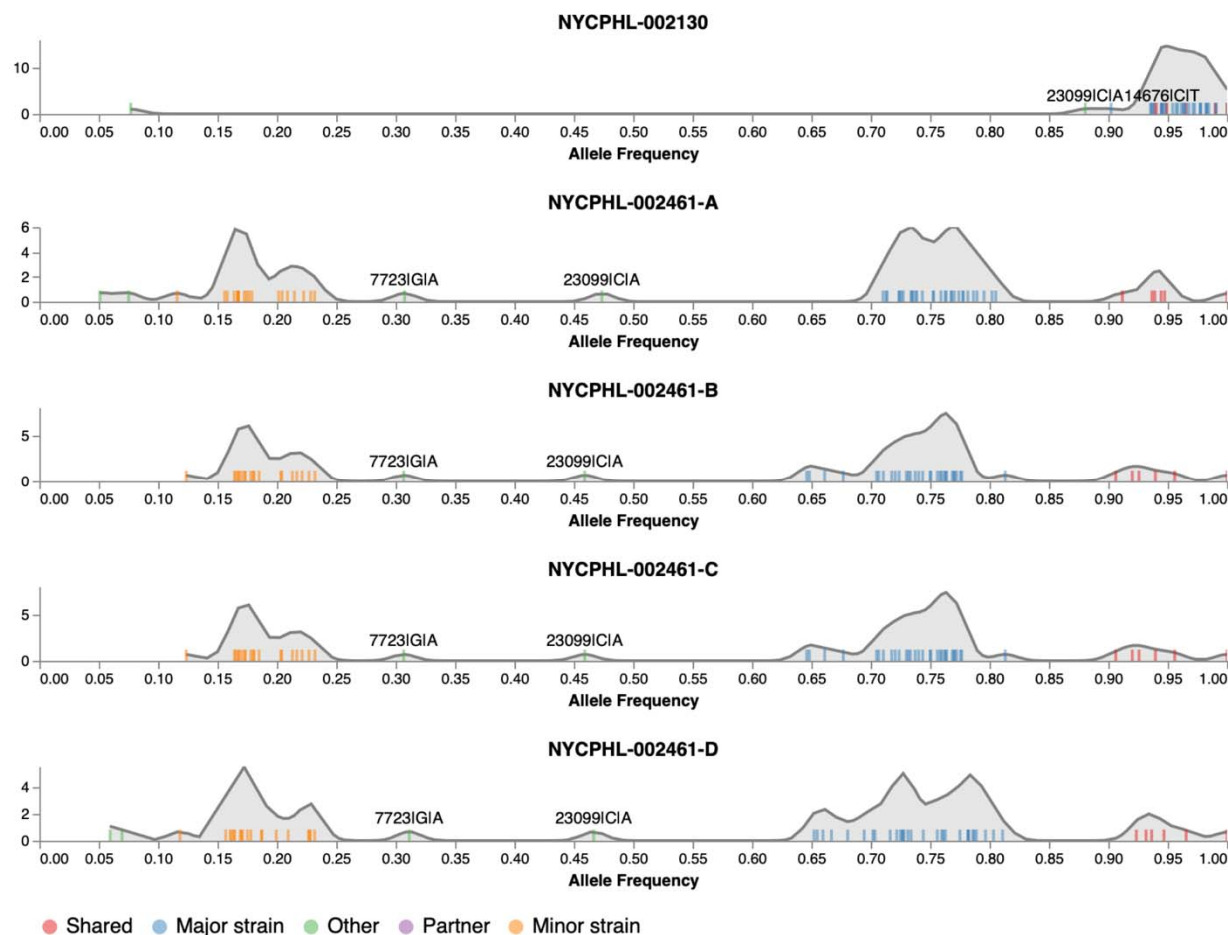
617

618 **Table 2: Four gamete recombination test results for 15 sets of aligned read fragments in**
 619 **the S (spike) and N (nucleoprotein) genes.**

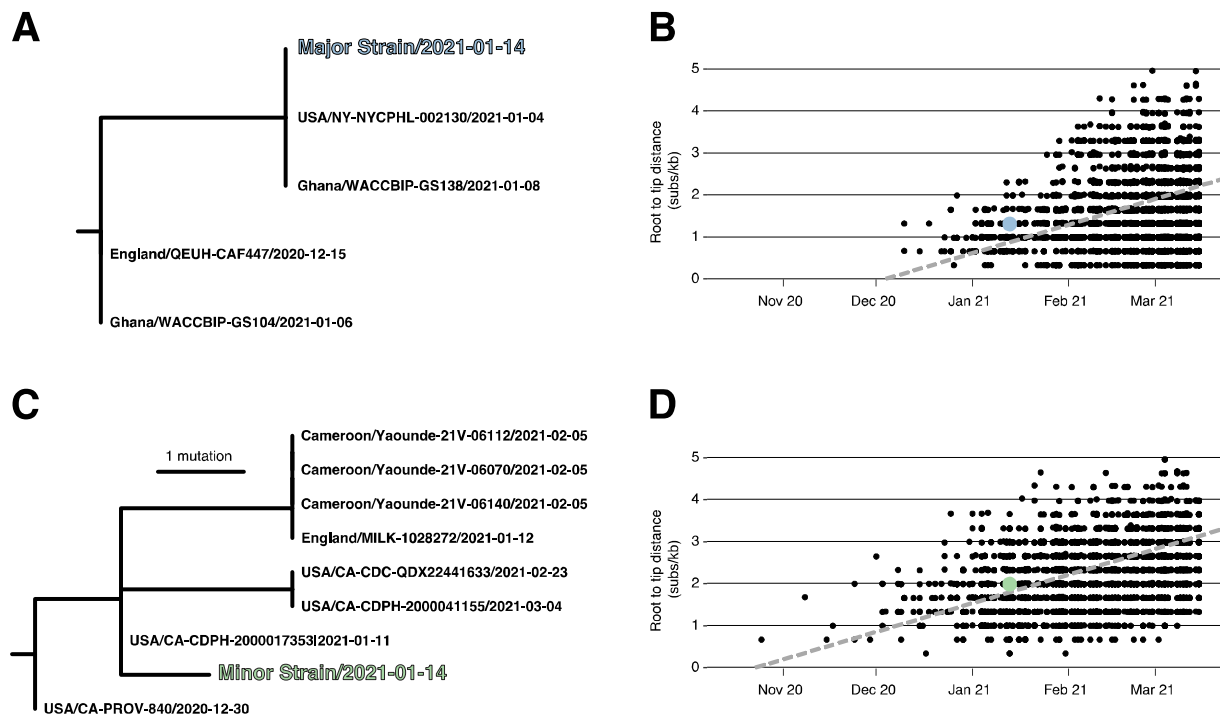
Gene	Fragment	Start ¹	End ¹	Recombination test <i>p</i> -value		
				PHI	MCL	R ² vs Dist
S	1	21354	21730	>0.9	>0.9	>0.9
	2	21658	22038	>0.9	>0.9	>0.9
	3	21962	22346	>0.9	>0.9	>0.9
	4	22263	22650	0.682	0.393	0.132
	5	22517	22903	>0.9	0.401	0.142
	6	22798	23212	<0.001	0.355	0.3
	7	23123	23522	>0.9	<0.001	0.005
	8	23444	23847	<0.001	0.317	0.008
	9	23790	24169	>0.9	0.047	0.03
	10	24079	24467	>0.9	0.003	<0.001
	11	24392	24789	<0.001	0.071	0.477
	12	24697	25076	0.741	0.155	0.208
N	1	28395	28779	0.491	0.482	0.459
	2	28678	29063	>0.9	0.868	0.628
	3	28986	29378	<0.001	<0.001	<0.001

620 ¹Position relative to the Wuhan-Hu-1 reference strain
 621

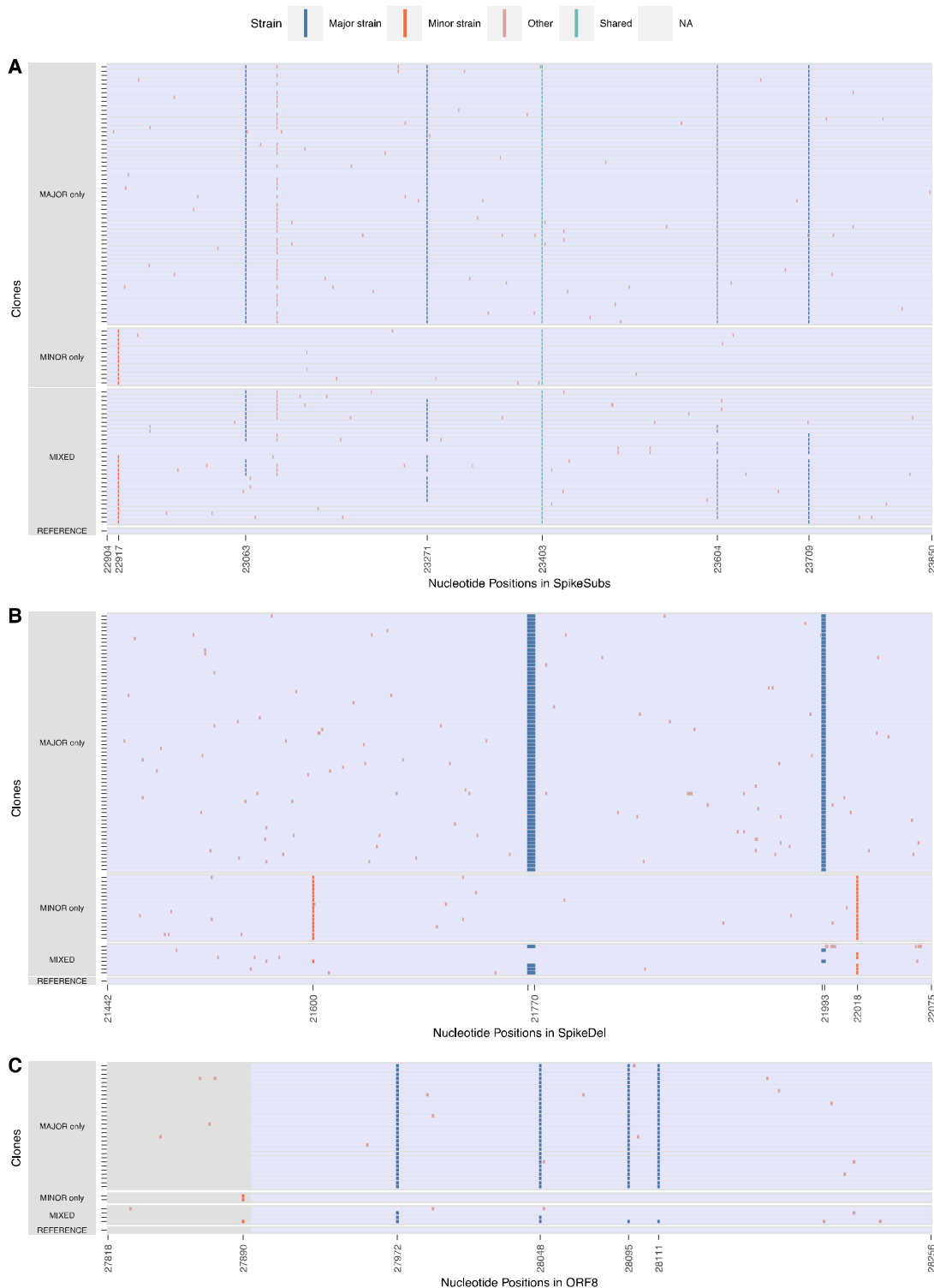
622 **FIGURES**
623



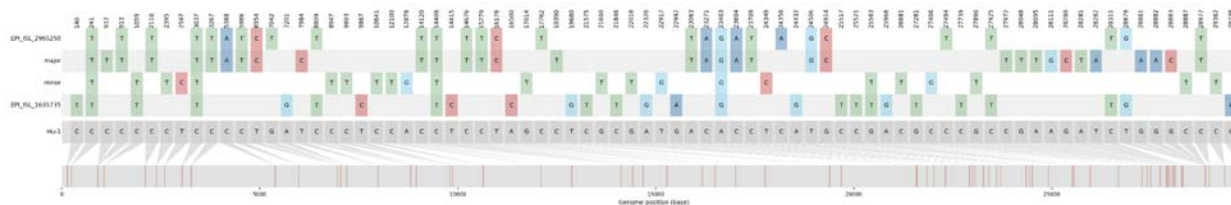
624
625
626 **Figure 1. The distribution of allelic frequencies in the index case (NYCPHL-002130) and**
627 **named partner with suspected superinfection (NYCPHL-002461).** Frequencies of individual
628 alleles shown as ticks, a smoothed kernel density plot is used to highlight clustering patterns,
629 and colors represent allele types.



630
 631 **Figure 2. Phylogenetic consistency of major and minor variants.** (A) Phylogeny of B.1.1.7
 632 immediate relatives, (B) Root-to-tip regression for B.1.1.7, (C) Phylogeny of B.1.429 immediate
 633 relatives, (D) Root-to-tip regression for B.1.429. NY-NYCPHL-0024661 is the genome deposited
 634 in GISAID from the case of putative superinfection.



635
 636 **Figure 3. Major, minor, and mixed alleles in cloned sequences.** Clones in S-substitution
 637 (S_Subs), S-Deletion (S_Del), and ORF8 were sequenced. Major and Minor allele positions are
 638 defined by the variant calling analysis performed on Galaxy. For each of the cloned region here,
 639 there are clones with only major alleles, minor alleles, and mix of both alleles. Out of the three
 640 cloned regions, the S-substitution clones has the highest frequency of mixed variants.



641
642 **Figure 4. The nucleotide variation present in the major, minor, and putative recombinant**
643 **strains.** The distribution of the nucleotide variation found in the major, minor, B.1.526
644 (EPI_ISL_1635735), and single putative recombinant (EPI_ISL_2965250) strains relative to the
645 reference genome (Wuhan Hu-1; bottom grey sequence).
646
647

648 **SUPPLEMENTAL TABLES**

649
 650 **Supplementary Table 1. Recombinant haplotype frequencies across separate extractions,**
 651 **reverse transcription, and PCR amplification in high-throughput sequencing for S-**
 652 **Substitution (S_Sub) region, nucleotide positions 23604 and 23709.**

653

Haplotypes			Count (Frequencies)			
Type	23604	23709	NYCPHL-002461-A	NYCPHL-002461-B	NYCPHL-002461-C	NYCPHL-002461-D
MAJOR	A	T	3633 (78.57%)	4095 (76.43%)	3778 (76.40%)	4745 (78.24%)
MINOR	C	C	634 (13.71%)	776 (14.48%)	762 (15.41%)	851 (14.03%)
MIX	A	C	162 (3.50%)	234 (4.37%)	191 (3.86%)	237 (3.91%)
MIX	C	T	195 (4.22%)	253 (4.72%)	214 (4.33%)	232 (3.83%)
Depth			4624 (100%)	5358 (100%)	4945 (100%)	6065 (100%)

654
 655
 656

657 **Supplementary Table 2. Recombinant haplotype frequencies across separate extractions,**
 658 **reverse transcription, and PCR amplification in high-throughput sequencing for ORF8**
 659 **region, nucleotide positions 27972, 28048, 28095, 28111.**

Haplotype	Positions				Count (Frequencies)			
	27972	28048	28095	28111	NYCPHL-002461-A	NYCPHL-002461-B	NYCPHL-002461-C	NYCPHL-002461-D
MAJOR	T	T	T	G	1382 (70.22%)	1164 (69.83%)	1110 (68.90%)	1873 (70.26%)
MINOR	C	G	A	A	381 (19.36%)	305 (18.30%)	347 (21.54%)	505 (18.94%)
MIX	T	G	A	A	57 (2.90%)	40 (2.40%)	31 (1.92%)	77 (2.89%)
MIX	C	T	T	G	50 (2.54%)	60 (3.60%)	55 (3.41%)	66 (2.48%)
MIX	T	T	A	A	40 (2.03%)	43 (2.58%)	28 (1.74%)	48 (1.80%)
MIX	C	G	T	G	34 (1.73%)	28 (1.68%)	18 (1.12%)	45 (1.69%)
MIX	T	T	T	A	8 (0.41%)	7 (0.42%)	6 (0.37%)	12 (0.45%)
MIX	C	G	A	G	4 (0.20%)	6 (0.36%)	4 (0.25%)	12 (0.45%)
MIX	T	G	T	G	6 (0.30%)	8 (0.48%)	7 (0.43%)	15 (0.56%)
MIX	C	T	A	A	1 (0.05%)	3 (0.18%)	3 (0.19%)	5 (0.19%)
MIX	C	G	T	A	1 (0.05%)	1 (0.06%)	NULL	NULL
MIX	T	T	A	G	1 (0.05%)	1 (0.06%)	2 (0.12%)	7 (0.26%)
MIX	C	T	A	G	1 (0.05%)	1 (0.06%)	NULL	NULL
MIX	T	G	T	A	1 (0.05%)	NULL	NULL	NULL
MIX	C	T	T	A	1 (0.05%)	NULL	NULL	1 (0.04%)
Depth					1968 (100%)	1667 (100%)	1611 (100%)	2666 (100%)

660
 661
 662
 663